Innovative Approach in the Diagnosis of Gliomatosis Cerebri Using Carbon-11-L-Methionine Positron Emission Tomography

Katsuyoshi Mineura, Toshio Sasajima, Masayoshi Kowada, Yoshiyuki Uesaka, and Fumio Shishido

Neurosurgical Service and Department of Pathology, Akita University Hospital, and Department of Radiology and Nuclear Medicine, Research Institute for Brain and Blood Vessels-Akita, Akita, Japan

A case of gliomatosis cerebri was studied with positron emission tomography (PET). Carbon-11-L-methionine (^{11}C-Met) accumulated in the diffusely infiltrative tumorous area more widely and accurately than the lesion detected by conventional x-ray computerized tomography (CT) or magnetic resonance (MR) imaging. Autopsy findings three months after the time of the PET study showed good anatomical correspondence between the extent of densely aggregated tumor cells and the region with high uptake of ^{11}C-Met. PET may offer an innovative approach in the delineation of gliomatosis cerebri, which has not been clearly recognized by CT or MR.

J Nucl Med 1991; 32:726–728

The growth pattern of gliomas is mainly divided into two major categories, consisting of infiltrative and relatively localized with an expansive character. The pattern is however heterogenous and varies widely among patients, according to tumor location and pre-existing brain structure (*1*). Gliomatosis cerebri, as first described by Nevin (*2*), is an extreme form of diffusely infiltrative growth of gliomas. Because of the lack of well-defined mass formation, neuroradiologic interventions such as x-ray computerized tomography (CT) and magnetic resonance (MR) imaging fail to provide the definitive diagnosis of this entity.

We report here anatomical correlation between the extent of tumor cells of gliomatosis cerebri, examined by pathologic study on the autopsied brain, and a lesion detected by carbon-11-L-methionine (^{11}C-Met) positron emission tomography (PET).

CASE REPORT

A 32-yr-old woman was admitted to the hospital with a 2-mo history of dizziness and unsteady gait. Her intelligence and cal-

culation had gradually retarded. CT of the head revealed poorly defined and extensive hypodense areas unassociated with a well-defined mass in the bilateral cerebral white matter. Mildly enhancing areas were present in the posterior paraventricular region, causing the ventricles displaced (Fig. 1).

T1-weighted (TR/TE=500/25 msec) MR images revealed a high-intensity signal in both parietal and temporal lobes with corpus callosum involvement. The lesions were not enhanced by gadolinium-DTPA. T2-weighted (1800/25) MR images showed bilateral hyperintensity dominant in the white matter (Fig. 1).

PET was performed using the Headtome III together with $C^{15}O_2$, $C^{15}O$, and ^{11}C-Met tracers. Regional cerebral blood flow (rCBF) and blood volume (rCBV) PET images depicted hyperperfused and highly vascular areas, respectively, in the bilateral temporal and parietal lobes. Peak values of rCBF and rCBV in the lesion indicated 111 ml/100 ml/min and 8.1 ml/100 ml, respectively, which were exceedingly higher than the mean values of rCBF (36.7 ml/100 ml/min) and rCBV (2.6 ml/100 ml) of both frontal gray matter. In PET images 45 min after an intravenous injection of ^{11}C-Met at a dose of 22.2 MBq/kg (0.6 mCi/
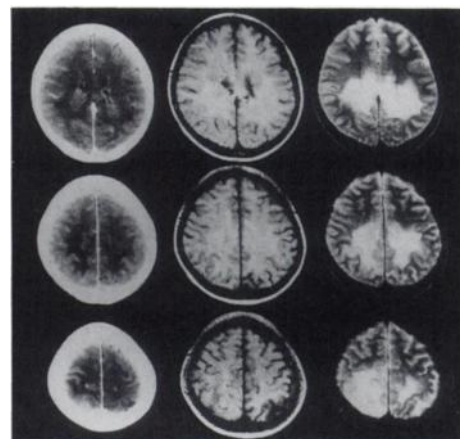

FIGURE 1. CT scans showed ill-bordered hypodense areas in the bilateral cerebral white matter with mildly enhancing paraventricular areas. T1-weighted, TR/TE=500/25 msec, and T2-weighted, 1800/25, MR images showed bilateral hyperintensity dominant in the white matter. (from left to right column: enhancing CT, T1-weighted MR, and T2-weighted MR: upper: the level through the corpus callosum, middle: the level of the centrum semiovale, lower: the level through the upper parietal lobe).

FIGURE 2. The region with increased uptake of the ^{11}C-Met tracer spread widely in the bilateral temporal and parietal white matter with the corpus callosum, and even extended to the temporal and occipital gray matter, which CT and MR did not detect as lesions. (A, B, and C represent ^{11}C-Met PET images through the corpus callosum, at the level of the centrum se-miovale, and through the upper parietal lobe, respectively, correspondingly to CT and MR imaging.)
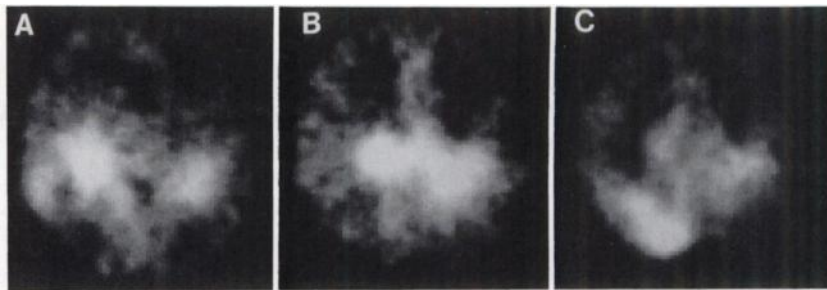
kg), the region with increased uptake of the tracer extended widely into the bilateral temporal and parietal white matter and even into the temporal and occipital gray matter together with the corpus callosum, which CT and MR did not detect as lesions. The ratio of tumor/non-tumor (T/NT) as an indicator of selective uptake in the tumor ranged from 2.4 to 3.0. The frontal gray matter was representative presumably, of nontumor regions (Fig. 2).

Specimens obtained from the right parietal white matter through a stereotaxic biopsy were diagnosed as infiltrative astro-cytoma.

A total dose of 60 Gy was postoperatively irradiated to the whole brain in conjunction with steroids and glycerol treatment. Nevertheless, neurologic symptoms and signs deteriorated pro-gressively during the radiotherapy over 6 wk, and at the end the patient became comatose with associated tetraparesis, predomi-nantly on the right side. Follow-up CT scans after completion of the therapy revealed extensive hypodense areas without mass formation in the bilateral white matter, similar to the preirradia-tion study.

Three months after the PET study, the patient died. Autopsy disclosed diffuse enlargement of both cerebral hemispheres and the brain stem was without a well-defined nodular mass. The tumor invaded mainly the white matter, and normal configura-tions of the subcortical nuclei such as the basal ganglia and the thalamus were relatively preserved. Microscopically, small round and ovoid gliomas cells with marked atypism widely and infiltra-tively spread in the entire cerebral hemisphere across the corpus callosum. Demyelinization and vacuolation, probably due to the radiotherapy, were evident especially in the white matter. The pathologic condition of tumor cell distribution was mainly clas-sified into three types as follows: (1) dense accumulation of tumor cells prominently around blood vessels or neurons, (2) diffuse infiltration of tumor cells along neuroglial fibers, and (3) subpial spread and superficial gray matter infiltration of tumor cells especially in the right temporal and occipital regions, where only ^{11}C-Met PET other than CT and MR detected significant abnor-malities. The histologic finding was typical of gliomatosis cerebri.

DISCUSSION

Symptoms and signs specific to gliomatosis cerebri are not apparent; usually symptoms are limited to raised in-tracranial pressure and change of character. CT findings of gliomatosis cerebri often seem normal, occasionally showing nonspecific abnormalities of small ventricles or ill-bordered hypodensity without mass effect. MR has been expected to be effective in visualizing lesions of gliomatosis

cerebri (3–5) because of high resolution. There is however no signal intensity pathognomic to this entity, and the differential diagnosis has remained uncertain among other brain tumors, brain edema, brain injuries, and degenera-tive diseases. Also, preserved normal brain structure, char-acteristic of this disease, prevents apparent differentiation from presenting lesions.

A number of PET studies have been clinically applied on the diagnosis of brain tumors from hemodynamic and metabolic aspects using various tracers including $C^{15}O_2$, $^{15}O_2$, $C^{15}O$, ^{18}F-fluorodeoxyglucose (FDG), and ^{11}C-Met (6–10). The ^{11}C-Met tracer is reported to be powerful in imaging cerebral gliomas because of high accumulation in the tumors as "hot" lesions (8,10), although the mecha-nism of ^{11}C-MET uptake and metabolism has remained speculative. Also, ^{11}C-Met can be an index of tumor ma-lignancy (6).

In the present case, CT could not recognize the deline-ation of gliomatosis cerebri even with contrast enhance-ment. T2-weighted MR imaging detected wide involve-ment of the bilateral white matter but failed to depict the lesion of subpial and superficial gray matter, probably
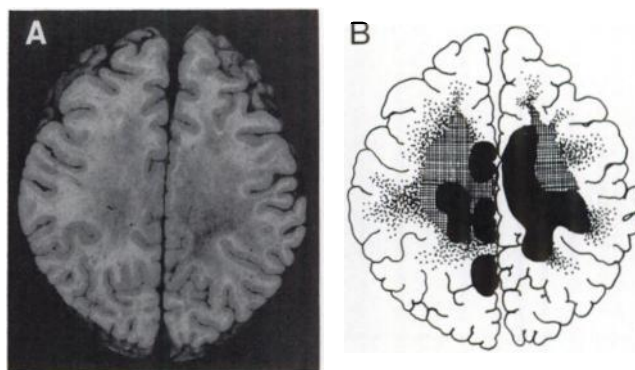
FIGURE 3. A cross-section (A) of the autopsied brain was obtained at a corresponding level to the plane of the PET image, as revealed in Figure 2B. The section included the following types of pathologic conditions (B): dense accumulation of undifferen-tiated tumor cells with perivascular and perineural arrangement (solid areas), tumor cells with marked vacuolation and demyelin-ization (lattice areas), and diffusely infiltrating tumor cells along neuroglial fibers (dots areas). The extent of high density of tumor cells correlated strongly with the high uptake region of the ^{11}C-Met PET image.

because the hyperintense signal of subarachnoid space overlapped the abnormal signal density of the lesion. In contrast, ^{11}C-Met PET images showed more extensive abnormalities than MR, although angulation of the section was modestly different. Carbon-11-L-methione has the advantages of radiologic augmentation as well as paucity of tracer accumulation in normal parenchyma for detecting subtle difference of tissue density of infiltrative tumors.

From the present topographic comparison, the tracer accumulated intensely in the superficial gray matter with tumor cell infiltration as well as areas with dense aggregations of tumor cells, as was shown in Figure 3. Lower accumulation was noted in the areas where disperse tumor cells infiltrated with centrifugal growth toward the cortex. Considering that the clinical symptoms and signs deteriorated progressively during the radiotherapy the tumor, mainly consisting of cells resistant to therapy, might proliferate uniformly. Configuration of the area with high uptake of ^{11}C-Met was proportional to the extent of tumor cells aggregations. Therefore, the area of ^{11}C-Met accumulation might be highly consistent with the distribution of tumor cells even at the time of the PET study.

REFERENCES

1. Scherer HJ. The forms of growth in gliomas and their practical significance. *Brain* 1940;63:1–35.
2. Nevin S. Gliomatosis cerebri. *Brain* 1938;61:170–191.
3. Romero FJ, Ortega A, Titus F, Ibarra B, Navarro C, Rovira M. Gliomatosis cerebri with formation of a glioblastoma multiforme. Study and follow-up by magnetic resonance and computed tomography. *J Comput Tomogr* 1988;12:253–257.
4. Schmidbauer M, Muller C, Podreka I, Mamoli B, Sluga E, Deecke L. Diffuse cerebral gliomatosis presenting as motor neuron disease for two years. *J Neurol Neurosurg Psychiatry* 1989;52:275–278.
5. Spagnoli MV, Grossman RI, Packer RJ, et al. Magnetic resonance imaging determination of gliomatosis cerebri. *Neuroradiology* 1987;29:15–18.
6. Derlon JM, Bourdet C, Bustany P, et al. [^{11}C]L-methionine uptake in gliomas. *Neurosurgery* 1989;25:720–728.
7. DiChiro G, DeLaPaz RL, Brooks RA, et al. Glucose utilization of cerebral gliomas measured by [^{18}F]fluorodeoxyglucose and positron emission tomography. *Neurology* 1982;32:1323–1329.
8. Ericson K, Lilja A, Bergstrom M, et al. Positron emission tomography with ([^{11}C]methyl)-L-methionine, [^{11}C]D-glucose, and [^{68}Ga]EDTA in supratentorial tumors. *J Comput Assist Tomogr* 1985;9:683–689.
9. Mineura K, Yasuda T, Kowada M, Shishido T, Ogawa T, Uemura K. Positron emission tomographic evaluation of histological malignancy in gliomas using oxygen-15 and fluorine-18-fluorodeoxyglucose. *Neurol Res* 1986;8:164–168.
10. Mineura K, Sasajima T, Suda Y, Kowada M, Shishido F, Uemura K. Early and accurate detection of primary cerebral gliomas with interfibrillary growth using ^{11}C-L-methionine positron emission tomography. *J Med Imag* 1989;3:192–196.

SELF-STUDY TEST
Gastrointestinal Nuclear Medicine
ANSWERS

in this case favor the diagnosis of hepatoblastoma. Although not considered in this instance, ^{67}Ga-citrate imaging also may be useful. However, some liver tumors, for example, hepatocellular carcinoma or lymphoma, may not be distinguishable from infections.

(Images courtesy of Dr. John H. Miller, Division of Nuclear Medicine, Children's Hospital of Los Angeles.)

References

1. Miller JH, Greenspan BS. Integrated imaging of hepatic tumors in childhood. Part I: malignant lesions (primary and metastatic). *Radiology* 1985;154:83–90.
2. Miller JH, Greenspan BS. Integrated imaging of hepatic tumors in childhood. Part II: benign lesions (congenital, reparative and inflammatory). *Radiology* 1985;154:91–100.